International Journal of Mechanical, Industrial and Aerospace Sciences
ISSN: 2517-9950
Vol:3, No:4, 2009

Cable Tension Control and Analysis of Reel Transparency for 6-DOF Haptic Foot Platform on a Cable-Driven Locomotion Interface

Martin J.-D. Otis, Thien-Ly Nguyen-Dang, Thierry Laliberté, Denis Ouellet, Denis Laurendeau and Clément Gosselin

Abstract—A Cable-Driven Locomotion Interface provides a low inertia haptic interface and is used as a way of enabling the user to walk and interact with virtual surfaces. These surfaces generate Cartesian wrenches which must be optimized for each motorized reel in order to reproduce a haptic sensation in both feet. However, the use of wrench control requires a measure of the cable tensions applied to the moving platform. The latter measure may be inaccurate if it is based on sensors located near the reel. Moreover, friction hysteresis from the reel moving parts needs to be compensated for with an evaluation of low angular velocity of the motor shaft. Also, the pose of the platform is not known precisely due to cable sagging and mechanical deformation. This paper presents a non-ideal motorized reel design with its corresponding control strategy that aims at overcoming the aforementioned issues. A transfert function of the reel based on frequency responses in function of cable tension and cable length is presented with an optimal adaptative PIDF controller. Finally, an hybrid position/tension control is discussed with an analysis of the stability for achieving a complete functionnality of the haptic platform.

Keywords—haptic, reel, transparency, cable, tension, control

I. Introduction

CABLE-DRIVEN parallel mechanisms are interesting for haptic applications allowing interactions between a user and objects in a virtual environment. The Cable-Driven Locomotion Interface (CDLI) under development in our laboratory includes two independent 6-DOF cable-driven haptic platforms for allowing users to walk on virtual terrain [1]. Its architecture is composed of motorized reels, cables used as the mechanical transmission, and the end-effector that provides the kinesthetic sensation to the user. Each cable actuator (refered to as the motorized reel) is composed of a DC motor with built-in quadrature position encoder, a strain gauge and a reel for applying cable tension, angular position or velocity control.

For such an application, the reel must be transparent to the user. Indeed, reel inertia, friction, non-linear strain gauge response, acquisition system precision and real cable behaviour such as elasticity and sagging can reduce the capability of the mechanism to reproduce the wrench involved in Haptic Display Rendering (HDR) with high fidelity [2]. Reel transparency is defined as the ability to which a force at the cable end can be guaranted for any cable and reel dynamics and therefore allow a large Z-width (impedance range) [3].

Hannaford uses a cable-driven mechanism for stability analysis of haptic interaction [4]. Other applications include fingertip grapsing [5] and touching [6]. Tension control is a challenging task because the sum of all cable tensions applied at the end-effector must balance the Cartesian wrench generated by a virtual environnment while considering the actual behaviour of the cables, reel friction and other non-linearities. Some cable properties for parallel mechanisms are presented in [7] as a means of describing geometrical sagging in static position control applications. Another reel design is presented in [8] for tension monitoring, but tension control for haptic display is not discussed. In fact, in some applications, it is possible to neglect reel and cable non-ideal effects like in [9] but in a large scale design such as the Cable-Driven Locomotion Interface [1] with high dynamics and impedance range, the transparency of each component must be modeled and compensated for by the control algorithm.

The motorized reel could be compared as a string musical instrument. Cable vibrations can actually enhance the undesirable effect of a typical PID motor controller that overshoots and oscillates radially and axially at a given natural frequency. In general, these phenomena only arise when actuation speed is high or the variation of cable tension increase abruptly. Hence, the dynamics of cable interference are not analyzed in the present work. Cable vibration analysis is presented in [10] and two controllers for reducing vibration in an elastic cable are developed in [11] and [12].

The second section of this paper presents the model of a cable for correcting the effective position of the mobile cable attachment point on the platform as a function of cable tension. The third section presents force feed-forward compensation seen at the cable attachment point for modelling cable sagging. The fourth section presents a design criterion for analysing the friction of the moving part. Finally, the last section presents the cable tension controller and the strategies for adjusting some parameters of the controller with Extremum Seeking-Tuning (ES-Tuning).

M. Otis, T.-L. Nguyen-Dang, D. Ouellet and D. Laurendeau are with the Electrical Engineering Department, Laval University, Quebec, Canada.

C. M. Gosselin and T. Laliberte are with the Mechanical Engineering Department, Université Laval. Clément Gosselin is a Professor and holds a Canada Research Chair in the Department of Mechanical Engineering at Université Laval in Québec City, QC, Canada (e-mail:gosselin@gmc.ulaval.ca).

This work was supported by the Natural Sciences and Engineering Research Council of Canada (NSERC). Martin J.D. Otis is a graduate student currently working on obtaining a Ph.D. degree at Université Laval in Québec City, QC, Canada.

A. The Geometry of the CDLI

As shown in Figure 1, the geometry of the CDLI is optimized to cover the largest workspace possible in a limited volume (i.e. the overall dimension of the complete CDLI) so as to avoid cable interferences and to minimize user interference with the cables while walking [1]. Note that due to the unilaterality of the actuation principle of a cable-driven mechanism [13], the geometry needs at least seven cables for controlling a 6-DOF platform. Since each platform has six DOFs for emulating human gait [14] and all cable attachment points are chosen so as to reach an optimal workspace, each haptic foot platform is actuated by eight cables.

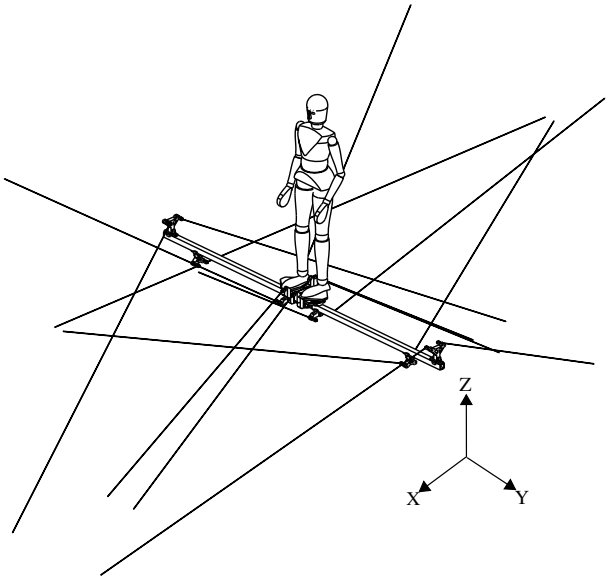

Fig. 1. CAD model of the complete CDLI (taken from [1])

B. Control Algorithm Strategy

The overall control for the CDLI is divided in four stages as described in Fig. 2. The first control stage is the stability controller as suggested in [15] and [16]. The second stage is the Cartesian haptic rendering [2]. This control accepts a wrench vector obtained from the contact between a foot and any virtual object as a constraint on each platform. This wrench applied on a platform is balanced with positive cable tensions using an Optimal Tension Distribution (OTD) algorithm described in [17], the result being a set of cable tensions, called the *setpoint*, that the cable tension controllers then attempt to maintain. The Cartesian pose of each platform can be estimated with the Direct Kinematic Problem (DKP) using the length of the cables (modeled by a straigt line without cable sagging) [18]. The third stage is the cable tension controllers and finally the current controllers for each motor. This paper describes the cable tension controllers with the calibration and optimisation procedure for a hybrid position/tension control.

C. Mechanical Reel Design

Each reel cable tension controller, being a part of the primary layer between the hardware and the overall control algorithm, must provide precise reel tension measurements as well as the real length of its deployed cable. Several non-ideal effects must therefore be modelled (at least partially), such as:

- the effect of gravity on each cable, as well as cable axial and radial stiffness, which not only influence the force directly applied on a foot platform, but also the cable length usually calculated from the motor quadrature encoders;
- the lateral displacement of the cable contact point on its winding drum, which shifts as a cable is rolled or unrolled due to the screw thread and its guide pulley;
- any residual feed-forward static friction forces between the deployed cable and the force strain gauge, usually caused by the presence of a mechanical part that acts as a static constraint point on the cable: these forces cannot be directly measured by the reel as they are *invisible* to the strain gauge. As a matter of fact, they cannot even be compensated for by an open-loop approach if no additional information about the user-applied forces are given during the Coulomb static friction regime. However, the dynamic feed-forward friction force can be taken into account during normal reel operation after the estimation of its corresponding Coulomb coefficient;
- the displacement of the force contact point between a cable and its strain gauge, which changes the Wheatstone bridge strain gauge response curve as a function of the normal cable tension.

Some of the above non-ideal effects can be minimized to the detriment of others by choosing a given reel design. For instance, it is possible to minimize the feed-forward friction forces by completely removing the static point constraint (eyelet), although this would limit the angle coverage of the reel beyond which not only the feed-forward friction forces would again become significant, but the variation of the position of the cable attachment point (which thereby limits the performance of an OTD algorithm controller that employs fixed attachment points) would also increase. In such a case, the internal friction forces of a strain gauge and the pulley friction forces still create an adverse feed-forward contribution that must be characterized in order to be indirectly compensated for by the CDLI controller (i.e. by using data from the 6-DOF wrench sensor). As a last resort, it is possible to change the mechanical design in order to eliminate both issues by using strain gauges directly on the platforms, but this ultimately results in a hardly generalizable mechanism (due to weight constraints) whose implementation would involve a costly wireless data transmission system.

For reducing acquisition and instrumentation systems as well as implementation cost, this paper proposes the use of a strain gauge mounted on the reel with 4-20mA amplifier as shown in Figure 3.

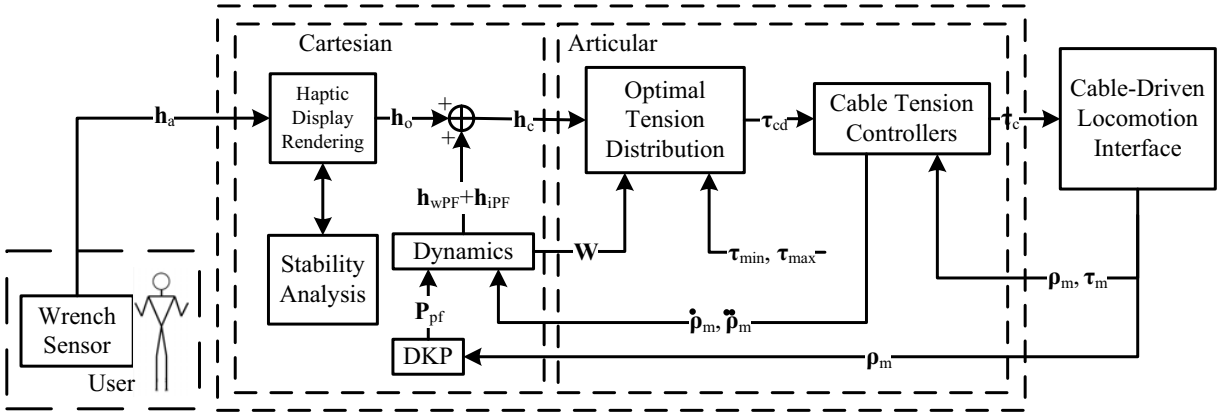

Fig. 2. Control algorithm process

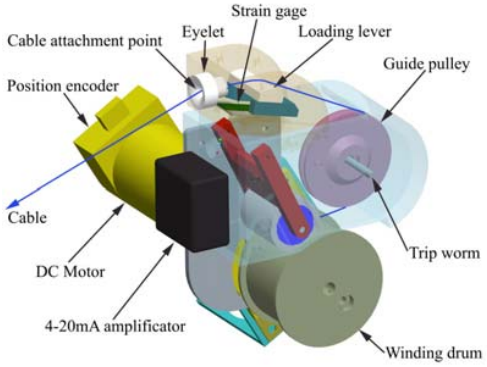

Fig. 3. CAD model of the motorized reel

II. Force and Position Correction

When modelling a cable-driven parallel mechanism system in order to properly employ an OTD algorithm, the cables are commonly regarded as being simple line segments unaffected by gravity. This is a valid approximation only when the following tension criterion described in [19] is satisfied, namely the *relative tension differential ratio*:

$$|\mathbf{T}_1| \geq \frac{\mu g \Delta s}{\beta} \tag{1}$$

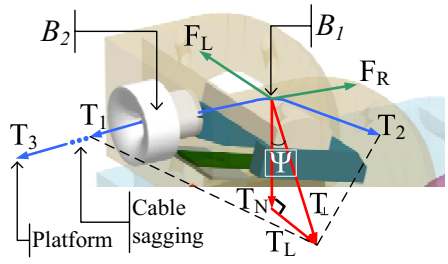

Fig. 4. Cable tensions and friction forces

where $|\mathbf{T}_1|$ is the cable tension at the cable attachment point as described by Fig. 4, g is the gravitational acceleration, $\beta \ll 1$ is the criterion parameter, Δs is the real cable length, and μ is an approximate constant linear cable density, which for a slightly sagging cable is defined as follows:

$$\mu \approx \mu_0 \left(1 + \frac{|\mathbf{T}_1|}{EA}\right)^{-1} \tag{2}$$

E being the cable Young modulus, A the cross-section, and μ_0 the cable linear density at rest. The OTD algorithm must then consider this constraint as a minimum cable tension parameter.

A. Gravity Position and Force Correction

The effect of cable sagging cannot be neglected when (1) is not satisfied, in which case it is still possible to correct for the Euclidean distance between a cable attachment point and its corresponding cable end-effector, knowing the tension vector at the cable attachment point. As a matter of fact, only three of the following variable quantities Δs, Δz, Δx, T_x, T_{1z}, T_{3z}, $|\mathbf{T}_1|$, $|\mathbf{T}_3|$ (respectively the cable length, its vertical-axis projection, its horizontal-axis projection, the horizontal component of the tension at the cable ends, the vertical component of the cable attachment point tension, the vertical component of the cable end-effector tension, the tension magnitude at the cable attachment point and the tension magnitude at its end-effector) are required to determine completely the spatial and tension properties of a given cable in static equilibrium, assuming that the effect of the non-ideal cable axial stiffness can be modeled by (2):

$$\left(\frac{\mu g}{T_x}\right)^2 \left((\Delta s)^2 - (\Delta z)^2\right) = 2\left(\cosh\left(\frac{\mu g}{T_x}\Delta x\right) - 1\right) \tag{3}$$

$$T_{1z} = \frac{\Delta z}{\Delta s}\left(|\mathbf{T}_1| + \frac{1}{2}\mu g \Delta z\right) - \frac{1}{2}\mu g \Delta s \tag{4}$$

$$T_x = \sqrt{|\mathbf{T}_1|^2 - T_z^2} \tag{5}$$

$$\Delta\mathbf{T} = \mathbf{T}_3 - \mathbf{T}_1 = [0, \mu g \Delta s]^T \tag{6}$$

where $\mathbf{T}_1 = [T_x, T_{1z}]^T$ and $\mathbf{T}_3 = [T_x, T_{3z}]^T$.

For the purpose of the cable tension controller, the CDLI controller is in charge of ensuring that condition (1) is met at all times, and (6) is thus used in conjunction with the position data from the CDLI controller to correct for the feed-forward tension difference in each cable due to gravity.

A more accurate equation could also be used to take into account the axial stiffness of the cable. It can be derived from a modified catenary cable differential equation using an infinitesimal formulation of (2):

$$\Delta z = \frac{1}{\mu_0 g}\left(|\mathbf{T}_3| - |\mathbf{T}_1| + \frac{1}{2EA}\left(|\mathbf{T}_3|^2 - |\mathbf{T}_1|^2\right)\right) \quad (7)$$

B. Variability of Strain Gauge Response

A cantilever strain gauge that deforms under a force applied normally at its centre usually has a calibration curve that can be approximated for most purposes by a second-order polynomial. However, in cases where this applied force is not a normal vector with respect to the strain gauge plane, the calibration curve changes shape as a function of the cable contact point position, and is thus prone to adverse hysteresis phenomena due to lateral static friction forces between the gauge interface and the cable. Even so, it is possible to use a simple bidimensional polynomial of order $2 \times N$ as a generalized calibration curve in the case where the lateral maximum Coulomb static force translates into a lateral maximum spurious cable folding angle that stays close to 0 degrees (i.e. nearly no folding at all).

III. Force Feed-Forward Compensation

In order to accelerate the reel response, three compensation blocks were added between the PID filter and the reel motor current controller, including a gravity force compensator (section III-A), a non linear reel friction compensator (section III-B), and a conventional reel inertia compensator which simply computes the equivalent *inertial torque* $T_m = J_m \alpha_m$, where T_m is the raw DC motor torque (i.e. without its gearbox of ratio N), J_m is the moment of inertia of the whole reel system (including the corresponding cable inertia as seen at the raw motor output as well as the pulley and rotor moments of inertia), and α_m is the raw motor angular acceleration.

Computing velocity and angular acceleration are challenging tasks due to encoder noise and shift in acquisition frequency. The problem comes from the computation of low speed movement when low resolution quadrature motor position encoders are used and from the interrupt handler latency (and/or operating system context switching). The choice of the numerical algorithm used to compute the derivatives of the force and position is critical because it not only determines the robustness of the system with respect to measurement noise, but it also limits the maximum response time of the controller. The optimization problem can thus be summarized as finding the best compromize between the accuracy of the derivative and both robustness and response time. All differential terms use a non linear time-varying algorithm similar to the one proposed in [20]. Indeed, inertial compensation computes motor acceleration with non linear double derivative of position that introduce hysteresis thresholding, similar to the Canny [21] edge detection algorithm, which has some adaptability to the local content of the data.

A. Gravity Force Compensation

It is still possible to accelerate the reel response by calculating a cable gravity force based on the cable spatial configuration. The force difference component that influences cable tension at its attachment point stems from the magnitude of the vector tension difference between the cable ends, as the latter corresponds to the difference between the vertical component of both tension vectors, as shown in (6), and is physically intuitive as it corresponds to the net weight of the deployed portion of the cable. This magnitude is multiplied by a weighting term $\cos\psi$, where ψ is the angle between the cable attachment point force vector and the gravity force vector (the orientation convention being determined so that the compensator *pulls* on the cable when the latter points downward). Therefore:

$$-F_g = (\mu g \Delta s)\cos\psi = \mu g \Delta s \left(\frac{T_{1z}}{|\mathbf{T}_1|}\right) \quad (8)$$

Combining the definition in (8) with (5), the following compensation force is obtained:

$$-F_g = \mu g \Delta z \left(1 + \frac{1}{2}\frac{\mu g \Delta z}{|\mathbf{T}_1|}\right) - \frac{1}{2}\frac{(\mu g \Delta s)^2}{|\mathbf{T}_1|} \quad (9)$$

As defined by (8), F_g cannot be greater than $\mu g \Delta s$ (in this case, the cable is parallel to gravity and then $\Delta z = \Delta s \Rightarrow T_{1z} = |\mathbf{T}_1|$). As $|\mathbf{T}_1|$ could be very low when the reel dynamic cannot follow the cable tip displacement (when the reel reaches its maximum speed or when the acceleration approaches its expected value), a limit must be imposed on the control law to avoid over estimation of gravity force compensation.

B. Non Linear Friction Compensation

A PID controller usually compensates for the viscous (and linear) component of the total friction forces acting on the process to be controlled. However, it can be beneficial to include a feed-forward compensator using a non linear model that at least combines Coulomb static and dynamic friction effects. This is why the friction model that was integrated in the force controller as a feed-forward compensator is similar to the known Dahl model whose parameters are derived from a more complete LuGre model [22]. This model is determined by an error-minimization algorithm in order to fit the velocity graph of an unloaded reel under a known ramp command, the theoretical description of which is described in [23]. In short, the Dahl equation (without the viscous friction term) for real-time non-linear friction compensator is:

$$F_{fi} = \left(f_c + (f_s - f_c)e^{-\left(\frac{v}{v_s}\right)^2}\right)\mathrm{sgn}(v) \quad (10)$$

where f_c is the dynamic Coulomb force, f_s is the Stribeck coefficient, v is the cable winding velocity, and v_s is the

characteristic Stribeck velocity. Note that in practice, the tuned values correspond to their angular counterparts as measured at the motor output.

IV. Friction Performance Analysis

It is possible to further improve the friction compensation by including the predictable static and dynamic components of the eyelet-induced friction forces that must be added outside of the controller feedback loop so as to account for its *invisibility* with respect to the measured strain gauge signal. Its determination can be achieved using a two-reel automated measurement method, where a strain gauge calibrated reel is used not only to determine the strain gauge calibration curve of all other reels, but also to calculate the forward reel Coulomb static and dynamic friction coefficients, assuming that the coefficients for all reels are nearly the same.

The next subsections describe the novel method for the calibration of the reels. First, the description of the friction model is presented for the calibration curve. After, this model is used for defining a performance index on the static transparency of the reel presented in section IV-E.

A. Eyelet relative coordinate system

A polar-like coordinate system can be implemented in the force controller to simplify the determination of the tension vectors of a cable between the reel eyelet because the latter can be considered in first approximation as an isotropic point constraint. Let $\mathbf{N}$ be the normal vector pointing outward that defines the eyelet symmetry plane, γ the angle between the external cable tension vector $\mathbf{T}_1$ and its internal counterpart $\mathbf{T}_2$, θ_1 the angle between $\mathbf{T}_1$ and $-\mathbf{N}$, θ_2 the angle between $\mathbf{T}_2$ and $+\mathbf{N}$, ϕ_1 the angle between the projector of $\mathbf{T}_1$ on the plane $\mathbf{N}$ and a reference vector $\mathbf{r}$ that lies on the aforementioned plane, and ϕ_2 the angle between $\mathbf{r}$ and the projector of $\mathbf{T}_2$ on the plane $\mathbf{N}$. The following definitions must then hold:

$$\mathbf{P}_1 = [\cos\phi_1 \sin\theta_1, \sin\phi_1 \sin\theta_1, -\cos\theta_1]^T \quad (11)$$

$$\mathbf{P}_2 = [\cos\phi_2 \sin\theta_2, \sin\phi_2 \sin\theta_2, \cos\theta_2]^T \quad (12)$$

therefore:

$$\cos\gamma = \mathbf{P}_1^T \mathbf{P}_2 \quad (13)$$

B. Coulomb friction at eyelet and at loading lever

In order to shorten the mathematical details behind the friction forces at the reel eyelet (point constraint) or at the strain gauge (line constraint), it is worth noting that the line constraint model can be applied to the point constraint situation simply by ensuring that, for a given static equilibrium configuration, the line constraint is perfectly collinear with vector $(\mathbf{P_1} \times \mathbf{P_2})$. To ensure static equilibrium, the following equations must hold:

$$|\mathbf{T}_L| = |\mathbf{T}_\perp| \sin\Psi = |\mathbf{F}_L| \quad (14)$$

$$|\mathbf{T}_1| = |\mathbf{T}_2| - |\mathbf{F}_R| \quad (15)$$

$$|\mathbf{T}_N| = |\mathbf{T}_\perp| \cos\Psi \geq \sqrt{\left(\frac{|\mathbf{F}_R|}{C_R}\right)^2 + \left(\frac{|\mathbf{F}_L|}{C_L}\right)^2} \quad (16)$$

where C_R, the static Coulomb friction coefficient in the direction of $|\mathbf{F}_R|$, and C_L, the static Coulomb friction coefficient in the direction of $|\mathbf{F}_L|$, are separated to account for the possible heterotropy of friction forces on the strain gauge. It is always possible to define a reference frame in which:

$$\mathbf{T}_2 = |\mathbf{T}_2|[1,0]^T,\ \mathbf{T}_1 = |\mathbf{T}_1|[\cos\gamma, \sin\gamma]^T \quad (17)$$

Thus:

$$|\mathbf{T}_\perp| = |\mathbf{T}_1 + \mathbf{T}_2| \quad (18)$$

$$= \sqrt{|\mathbf{T}_1|^2 + |\mathbf{T}_2|^2 + 2|\mathbf{T}_1||\mathbf{T}_2|\cos\gamma} \quad (19)$$

C. Cable tension differential

It is also possible to approximate the cable tension differential caused by the eyelet and the loading lever contact points. In fact, if $|\mathbf{T}_L| = 0$, then:

$$|\mathbf{F}_R| = C_R |\mathbf{T}_\perp| \quad (20)$$

Combining (15), (19) and (20), the following equation is obtained:

$$|\mathbf{T}_2| - |\mathbf{T}_1| = C_R \sqrt{|\mathbf{T}_1|^2 + |\mathbf{T}_2|^2 + 2|\mathbf{T}_1||\mathbf{T}_2|\cos\gamma} \quad (21)$$

Squaring this equation yields a quadratic equation in $\mathbf{T}_1$:

$$|\mathbf{T}_1|^2 + |\mathbf{T}_2|^2 - 2|\mathbf{T}_1||\mathbf{T}_2|\Gamma = 0 \quad (22)$$

whose solution is:

$$|\mathbf{T}_1| = B|\mathbf{T}_2|, \text{ with} \quad (23)$$

$$B \equiv \Gamma - \sqrt{\Gamma^2 - 1} \text{ and} \quad (24)$$

$$\Gamma \equiv \frac{1 + C_R^2 \cos\gamma}{1 - C_R^2}. \quad (25)$$

The negative root of (22) being dismissed because $\Gamma \geq 1$ while the condition $B \geq 0$ must be satisfied at all times. Note that the value of B might vary as a function of the applied cable tension for many reasons, among which:

- The fact that it is not necessarily the higher static friction hysteresis threshold that will be measured. In effect, if the force controller *leads* the position controller, then the latter must cancel the spurious velocity due to the tension transient between each force constant setpoint, thereby stabilizing the system at a tension slightly higher than the force controller setpoint minus the forward dynamic friction forces. To remedy the situation, it is possible to use a velocity controller with a setpoint $\omega = 0$ instead of a position controller, which ensures an absence of oscillatory motion due to the position controller reacting to the force setpoint. Moreover, to ensure that the higher static friction threshold is measured accurately,

a negative force ramp contribution $F_{\angle} = -\varsigma t$ can be added in a feedforward manner to the speed controller after stabilization at $\omega = 0$ (t being defined so that stabilization occurs at precisely $t = 0$) to measure the breakout tension, which occurs as soon as the state of the position encoders change. Note that the slope of this ramp must be chosen so that the tension variation cause negligible measurement delay due to the response time τ of the reel. In other terms, $\varsigma \ll \tau^{-1}$;
- The possibility that the static friction coefficient increases with the adherence time between the two involved surfaces (see [24]).

The method can be generalized to the dynamic friction case by controlling the second reel using a velocity controller at a given setpoint, by repositioning the reel to its initial position for each measurement so as to minimize the error caused by the pulley lateral displacement, and by ensuring that the maximum cable folding angle ϑ_m stays negligible. However, the so obtained B values will then depend on the chosen setpoint, because the total kinetic friction coefficient not only depends on the Coulomb normal force-dependent contribution, but also on a linear velocity-proportional friction term as well as on non-linear effects at low velocity regimes (i.e. when the velocity setpoint is close to the Stribeck velocity).

Note that the mathematical derivations above assume the presence of only one forward friction contact point per reel, namely the eyelet contact point. However, the mathematical extension to multiple contact points is quite straightforward, if the friction coefficient for each contact point is the same. For instance, in the case of N contact points, if B_k is the friction *attenuation ratio* for contact point k, then it is possible to calculate an equivalent attenuation ratio using the following formula:

$$B_{eq} = \prod_{k=1}^{N} B_k \tag{26}$$

The dynamic friction counterpart of the *attenuation ratio* can also be determined similarly.

D. Two-Reel Determination of Friction Coefficients

The 2-reel method allows the evaluation of B, after which C_R can be evaluated by solving (25) using standard algorithms such as Newton-Raphson.

Consider two reels X and Y that are positioned face-to-face, and that have the exact same static friction *attenuation ratio* B (see section IV-C for details). Note that X and Y must allow both position and force control. For ensuring maximum accuracy, each position controller must be tuned to minimize overshoot, as this would cause errors due to the static friction hysteresis phenomenon. In the case of a PIF position controller, one can ensure minimum overshoot by reducing its response speed.

Here are the steps that must be repeated for different setpoints in order to obtain an accurate friction force curve that will subsequently allow a determination of the friction coefficient using quadratic regression that is robust to noise, and allows the characterization of any deviation from Coulomb's dry friction law (for instance, if a quadratic equation can be fitted to the friction coefficient curve instead of the usual linear curve, then B will vary linearly with the force setpoint applied to the controller of X) :

- Assign a force controller to X, and a position controller to Y;
- Initialize X with a given tension setpoint (represented by value x_1), and a default position setpoint for Y and then calibrate the strain gauge of Y with the y_1 value read so that its strain gauge reads the exact same value (x_1);
- Assign a position controller to X and a force controller to Y;
- Initialize X with a default position setpoint and Y with the exact same setpoint x_1. Note that the actual force applied by this reel will be in fact $B^2 x_1$, whereas the apparent force read by the software will be simply x_1;
- Read the force measured by the strain gauge of X (value x_2). This value, which is accurate because the strain gauge is calibrated, should be: $x_2 = B^4 x_1$. Therefore, B can be simply deduced by calculating $B = (x_2/x_1)^{1/4}$;
- Compute the new calibraion curve with the real tension value $y_2 = B x_2$.

This method can be generalized to the dynamic friction case by controlling the second reel using a velocity controller at a given setpoint, by repositioning the reel to its initial position for each measurement so as to minimize the error caused by the pulley lateral displacement, and by ensuring that this displacement stays negligible. However, the obtained B values will then depend on the chosen setpoint, because the total kinetic friction coefficient not only depends on the Coulomb normal force-dependent contribution, but also on a linear velocity-proportional friction term as well as on non-linear effects at low velocity regimes (i.e. when the velocity setpoint is close to the Stribeck velocity).

E. Two-Reel Transparency

The reel X gives N setpoints x_1 and the other reel measures y_1 which gives B_i for each setpoint as shown in Fig. 5. The definition of a performance parameter comes from the need for controlling the same tension in both reels. Then, computing the logarithm mean $\overline{\chi}$ and the logarithm standard deviation $\sigma(\ln B_i)$ of B_i provides an intersesting evaluation of reel performance. The design process of a prototype should include the minimization criterion in (27).

$$\min \quad \sqrt{\frac{\sum_{i=1}^{N} (\ln B_i - \overline{\chi})^2}{N}}, \text{ with} \tag{27}$$

$$\overline{\chi} \quad = \quad \text{mean}(\ln B_i). \tag{28}$$

For the static transparency of the reel, it is possible to define a criterion from the Weber's law [25] with (29) where the results are shown in Fig. 6. These results show that the performance of the reel decreases with an increase of the tension setpoint.

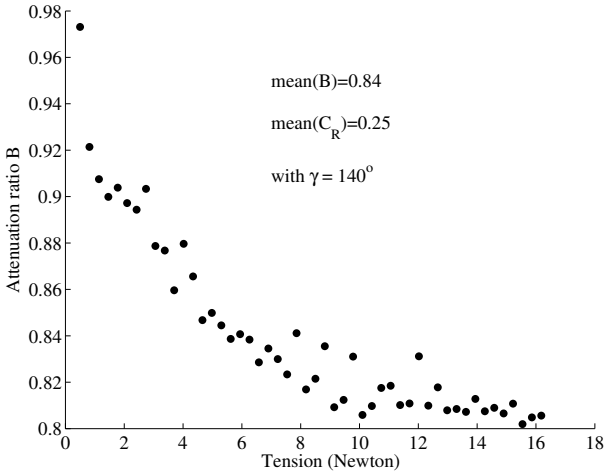

Fig. 5. Attenuation ratio in function of the tension setpoints

$$\frac{|\mathbf{F}_R|}{|\mathbf{T}_2|} = C_R\sqrt{1+B(1+2\cos\gamma)} < 0.1 \qquad (29)$$

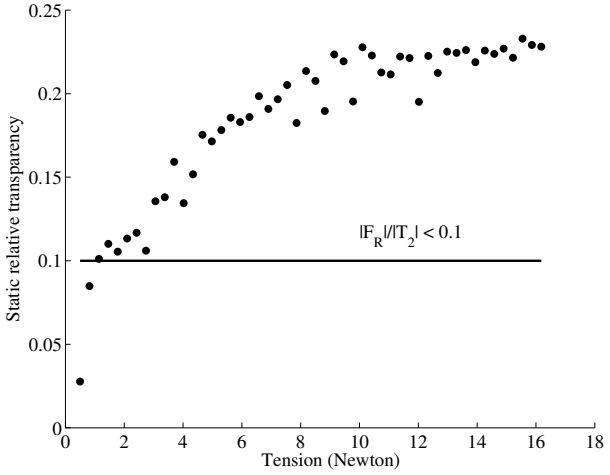

Fig. 6. Evaluation of static transparency

V. Cable Tension Controller Architecture

Fig. 7 shows the choosen architecture that aims at overcoming the non-linearity of the parameters. Two control types are implemented for achieving a complete functionnality wenever the platform is outside the workspce or the OTD algorithm could not find a solution for the prescribed wrench. The position controller is used to bring the walker from the initial position toward the centre of the workspace where the control is changed in tension. The selection of the control type is achieved automatically by the S matrix for each motor of the platform. This S matrix depends on the dynamic workspace determined by the OTD algorithm and the cable tensions.

This hybrid control could maintain the platform at the boundary of the workspace. At this position, the wrench sensor could be used for moving the platform outside the workspace as described in [26]. The transition between the boundary and the workspace is achieved by considering the minimum cable tension τ_{min} or with the wrench sensor for avoiding the platform to stick at this position :

- when the OTD cannot find a solution for the cable tensions, the control has to switch to the position control mode;
- when the position control mode is activated, the wrench sensor could move the platform;
- when the cable tension is under the minimal tension, the control have to switch to the tension control mode for avoiding excessive cable sagging;
- when the OTD finds a solution the control has to return in tension control.

The output of the tension controller is fed into a current controller that is linearized by a software implementation using polynomial least-squares regression represented by C_1. The latter approach provides a very efficient method for evaluating the linearizing function without consuming as much memory and processor time as a trilinear interpolated lookup table. The current controller runs on specialized hardware separate from the main control computer, and its response speed and range implies that it is acceptable to ignore the effect of the inductance of the reel DC motor, which greatly simplifies transfer function calculations. Finally, the data from the strain gauge is acquired, and a curve determined from quadratic least-squares regression is used to transform the raw sensor values into force (and thus torque) values represented by C_2. Also, a runtime error (RTE) process is implemented for ensuring security for the walker.

A. Reel Transfer Function

The non-instantaneous response measured at the strain gauge for a Heaviside-like setpoint curve is mainly due to the elastic properties of the strain gauge itself combined with the inertia of the reel drum and motor as well as the *parasitic* elastic contribution of the reel structure and the finite Young modulus of the affixed cable.

As the strain gauge has negligible mass in comparison to the reel drum and the DC motor rotor component, it is possible to include the effects of its elasticity and the cable elasticity within an effective Hooke constant which, combined with the inertia of all moving rotational parts (including the cable itself) allows the calculation of an approximation of an underdamped standard second-order transfer function that can be used to model system response at frequencies lower than the strain gauge resonant frequency.

The effective Hooke constant is determined by measuring the resonant frequency $\omega_R = 2\pi f_R$ of the system from a frequency response, in which case:

$$k_m = \frac{b_m^2}{2J_m} + J_m\omega_R^2 \qquad (30)$$

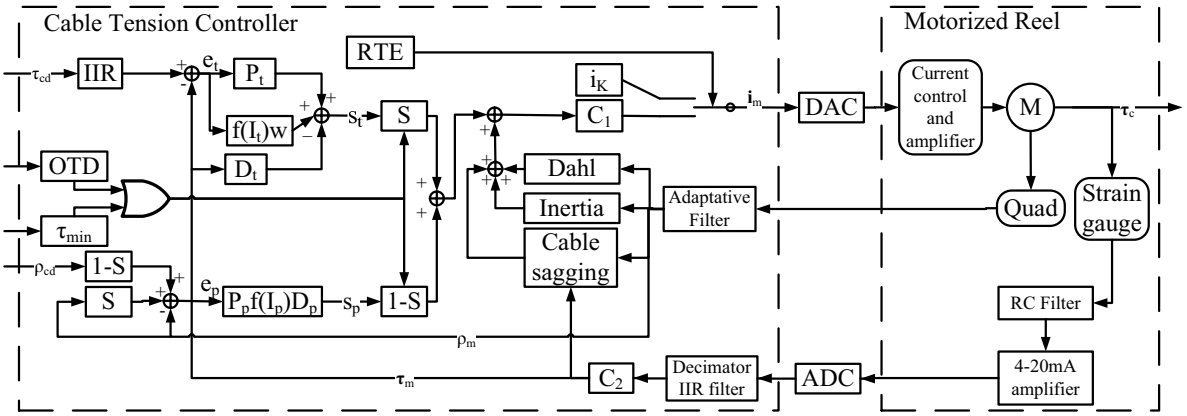

Fig. 7. Cable tension controller

where b_m is the effective viscous friction constant, J_m is the total rotational inertia reflected to the motor axle and k_m is the effective Hooke constant.

The transfert function of the reel could be compared to a string instrument where the natural frequency f_n is determined by the tension and the lenght of the cable computed with (31) for an infinitly flexible cable [27].

$$f_n = \frac{n}{2\Delta s}\sqrt{\frac{|\mathbf{T}_1|}{\mu}} \tag{31}$$

where Δs is the cable length, $|\mathbf{T}_1|$ is the cable tension outside the reel (after the eyelet) and μ is an approximate constant linear cable density. The next analysis considers a variation factor of two for the cable length Δs and the square of the tension $\sqrt{|\mathbf{T}_1|}$ for determining the influence of these parameters on the reel transfert function.

Fig. 8, 9 and 10 show the pratical bandwidth of the reel in function of the cable length and the tension. These results demonstrate that the reel does not respond as a string instrument and the cable length has a proportional influence on the damping of the transfert function as expected by the (31). Indeed, the optimal control needs an adaptative PIDF controller to take account of the cable length.

These frequency response curves not only show the main resonance peak at very low frequencies corresponding to the mass-spring system of the overall structure, reel drum and the strain gauge Hooke constant, but also a small high-frequency resonance peak near the Nyquist frequency (316 Hz) of the system, which can be explained as the uncoupled vibration of the strain gauge itself. As such, a better model to be used would be a higher-order transfer function, but this is ignored, as the final optimization of the FPID parameters of the reel controller will be achieved using the ES-Tuning algorithm.

This model proposed in (30) is used as a starting point for determining initial PID parameters using [28] before automatic tuning during the calibration procedure with an ES-Tuning algorithm [29] presented in the section V-C. The ES-Tuning algorithm is well suited to find the optimal controller and then define the adaptative control law inside the PIDF.

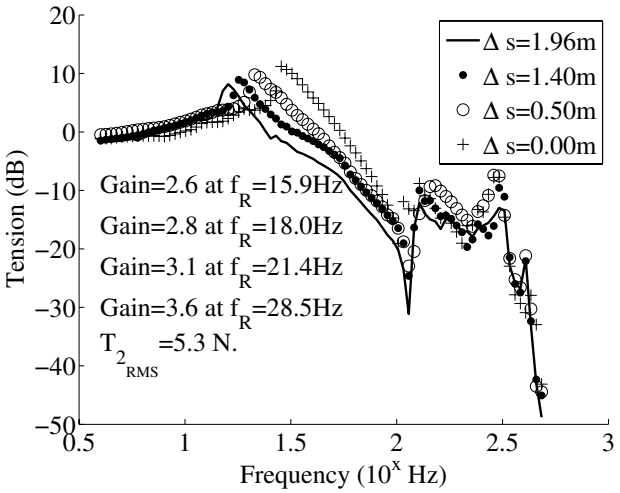

Fig. 8. Bandwidth of the reel for a constant tension and four cable lengths

B. Internal Closed-loop Control Architecture

The chosen force controller architecture is based on a slightly modified PID closed-loop control scheme as described in [29] that includes all feed-forward compensation terms explained above as well as an open-loop (and optional) setpoint filter, and whose core can be detailed as follows. Within the Laplace domain, let G be the process to be controlled, C_y a controller term, and C_r its *derivative-reduced* counterpart:

$$C_y(s) = K\left(1 + \frac{1}{T_i s} + T_d s\right) \text{ and} \tag{32}$$

$$C_r(s) = K\left(1 + \frac{1}{T_i s}\right) \tag{33}$$

where the three PID coefficients are $P = K$, $I = K/T_i$ and $D = KT_d$. The servo system is designed such that the closed-loop transfer function $T(s)$ becomes:

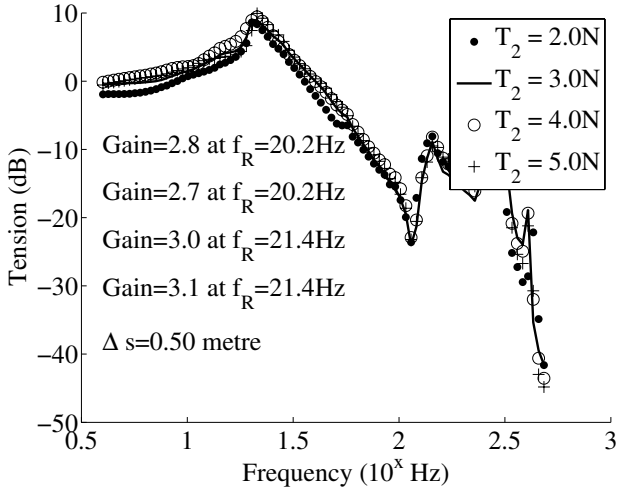

Fig. 9. Bandwidth of the reel for a cable length of 0.5 meter and four cable tensions

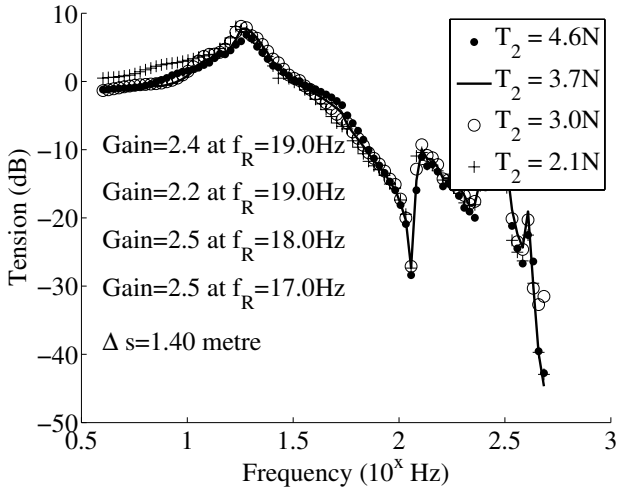

Fig. 10. Bandwidth of the reel for a cable length of 1.4 meter and four cable tensions

$$T(s) = \frac{GC_r(s)}{1 + GC_y(s)} \tag{34}$$

This transfer function in (34) must be changed in practice so as to take into account the floating point calculation errors which increase monotonically with the magnitude of the numbers involved. In effect, Killingsworth suggests that controller C_r be inserted between the input of a closed-loop controller and a given setpoint r, which is numerically equivalent to calculating the effects of an open-loop integrator C_r, and then by compensating its asymptotic ever-increasing behaviour by subtracting another monotonically increasing integrator term C_y to it. Although it is always possible to implement a circular accumulator buffer in order to compensate for this behaviour, one can also notice that in the time domain, it is equivalent to calculate the derivative term separately from the integral and proportional terms of the PID controller, all within a standard PID architecture as described in Fig. 7.

From this architecture, the law governing the PIDF function of the cable length must be found. The derivative coefficient D from the choosen PIDF structure is used to give energy in the direction of the cable movement and help for compensating dynamic friction. This coefficient could be adjusted as a function of the velocity of the motor. From the bandwidth figures, the proportional coefficient P should always be close to one for all cable lengths. Then, only the integrator coefficient I should be adjusted online when the tension control is activated. The next section presents the relation of the adaptative law.

C. Tuning

The PID controller parameters are optimized by locally minimizing a cost function that describes the accuracy of the controller output with respect to a given Heaviside setpoint. Two methods are investigated within the framework of a real robotic device. A modified version of the ES-tuning algorithm described in [29] which calculates the gradient of the cost function using a combination of high-pass and low-pass digital filters in order to extract the information from sine modulation of the three PID parameters, and a standard algorithm that instead extrapolates this gradient using multidimensional least-square regression of a set of neighboring points in the PID parameter space. One expects the ES method to converge faster than the least-squares method, for the latter must poll a sufficient number of neighboring points to a given position in the PID parameter space in order to calculate its gradient. The discrepancy between the two methods was found to be experimentally quite small due to inherent measurement noise which favors robustness over convergence speed [30].

1) Cost functions: In a cable tension control application where the OTD algorithm adjusts the setpoint, overshoot should be avoided with a low damping response. A general rule in designing a meaningful cost function is usually to tune the settling time and the rise time of the controller response while minimizing overshoot. It is possible to combine both usual ISE and ITSE cost functions by using a sigmoid weighting function so that not only the transient portion is de-emphasized, but the subsequent settling phase basically corresponds to a constant weighing function, as in the ISE:

$$\eta(t) \equiv \frac{\left(ITSE + \frac{1}{t_s - t_0}\int_{t_0}^{t_s} \frac{1}{1+e^{\pi(t-t_s)/(2t_s)}}\epsilon^2 dt\right)}{\eta(O(1))}, \tag{35}$$

where $\eta(t)$ is the cost function, $\eta(O(1))$ is the cost function evaluated for a first order system, ϵ is the error between the cable tension command (the reference r) and the strain gauge measure (the output y), t_s is the settling time of the desired response and $\pi/2$ adjusts the curve of the sigmoid. This reduces the need for fine tuning the constant t_s to achieve the desired response. Instead, it is chosen as a value that is extrapolated directly from the natural oscillation frequency of the second-order model using the simple relation $t_s \leq 2\pi/\omega_n$. The conditions $\eta < \eta_{max}$ must be verified ensuring that the algorithm does not enter in a unstable region. η_{max} is determined experimentally.

η gives a measure on the haptic transparency and the performance of the reel with a consideration on the dynamic (settling time t_s) and on the cable tension error ϵ. The Fig. 11 gives the cost function evolution for optimizing the PIDF for the same cable length from the Fig. 8. The convergence of the ES-Tuning is thus influenced by the cable length as expected.

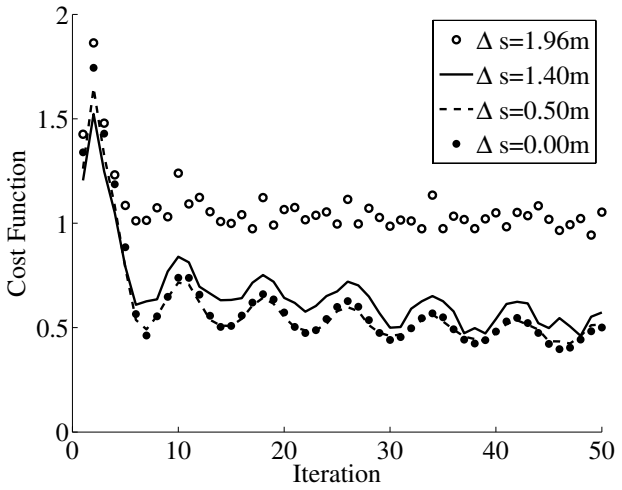

Fig. 11. Evolution of the cost function for different cable length

2) Real-time implementation of ES-Tuning: The modifications to the ES-Tuning algorithm stem from the necessity of adapting the theoretical simulated procedure of [29] to a real cable-actuated robotic system in which the imperfect repeatability of the reel output for a given setpoint translates into a cost function measurement noise that must be taken into account in order to ensure convergence to the desired local minimizer, among other things. The setpoint filter time constant is added as a tunable parameter so that the smoothness of the PID response can be adjusted depending on the cost function employed. To restrict the parameters to positive values and to allow their tunability for a wide range of starting parameter space coordinates, the logarithm of each parameter is fed into the tuning algorithm, as this eliminates the pathological behaviour for very small parameter values where the discretization step of the numerical gradient integrator becomes significant.

3) Adaptative Control Law: The enhanced ES-Tuning is applied for different cable length for finding the optimal local solution for the cable tension controller. Although only the integrator term varies as described in section V-B, any constraints are given to the algorithm which it tries to find the optimal parameters for each PIDF coefficients inside the controller. Fig. 12 clearly demonstrates that the integrator coefficient decreases as a function of the cable length. The relation between the cable length and the integrator coefficient is found using linear regression as shown in Fig. 13.

VI. Results

The compensation algorithms for increasing transparency were applied to the cables of two motorized reels. This

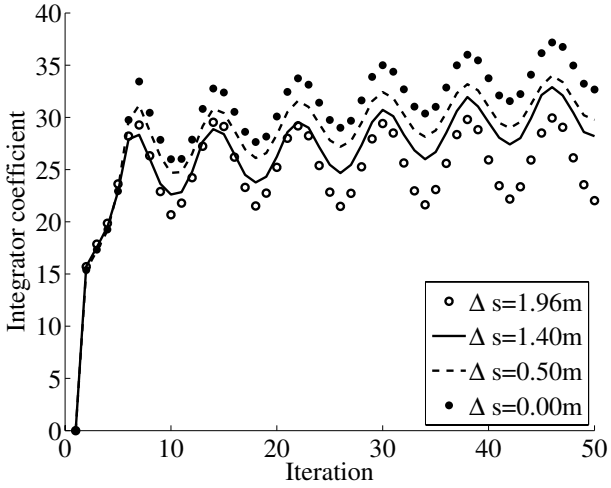

Fig. 12. Evolution of the integrator coefficient

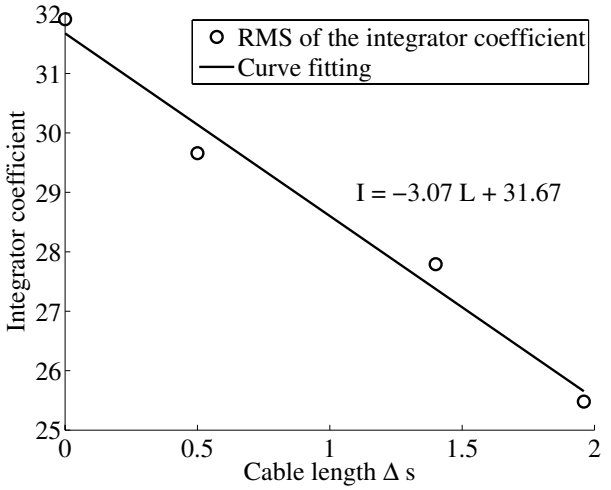

Fig. 13. Integrator coefficient as a function of the cable length

section presents some specific results obtain with the final design of the reel controller for improving the transparency. The first section described the problem met with the eyelet that cannot be compensated by the controller. The second section presents the force feed-forward compensation obtained from the analysis of the reel that aims to correct the tension hysteresis with the eyelet when the cable is moving. Finally, additional experiments are carried out with the hybrid control in order to gain further insight on the stability problem when the platform stays at the boundary of the workspace.

A. Tension hysteresis with the eyelet

Tension hysteresis between two reels should be very low and this curve is a direct consequence of the attenuation ratio B of (25). Hysteresis could occur between two reels when cable angle at the eyelet increases whenever using two materials with low static friction coefficient. This result cannot be compensated by the controller as the angle of the cable

with the afformentionned eyelet is not known and cannot be compensated with the attenuation ratio B. The resulting hysteresis, presented in Fig. 14, generates a force $|F_R|$, presented in (20), in the opposite direction of displacement when the cable is moved.

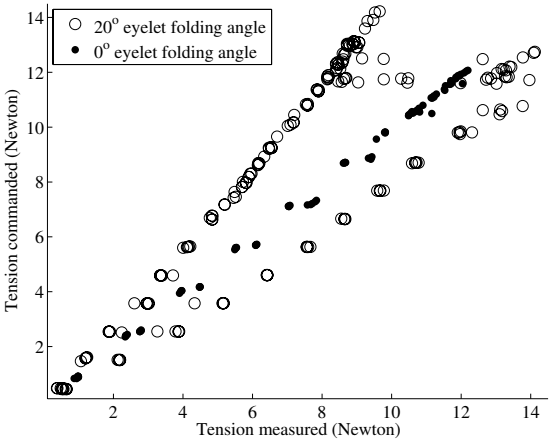

Fig. 14. Hysteresis in cable tension measurement

B. Force feed-forward compensation

Each component of the force feed-forward compensation (motor inertia, cable inertia/weight and friction) is plotted in Fig. 15 for a high amplitude sinusoid wrench command applied on the platform. The cable tip is attached to the haptic platform and can move freely. The same experiment with a low amplitude sinusoid wrench command is presented in Fig. 16.

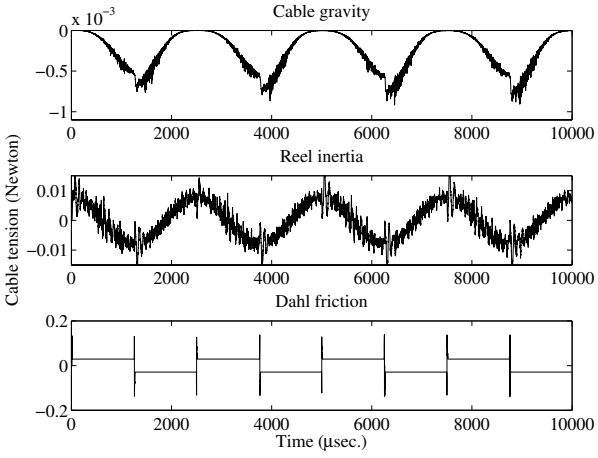

Fig. 15. Force feed-forward compensation with high angular velocity

Note that the computation of inertia at low speed is nearly impossible with a low resolution quadrature encoder (in fact, 2048 counts for a complete rotation). Then, compensation of inertia is activated only when the computed inertia reaches a noise floor limit. Some instability could occur when the estimated motor angular velocity is too noisy and the Dahl

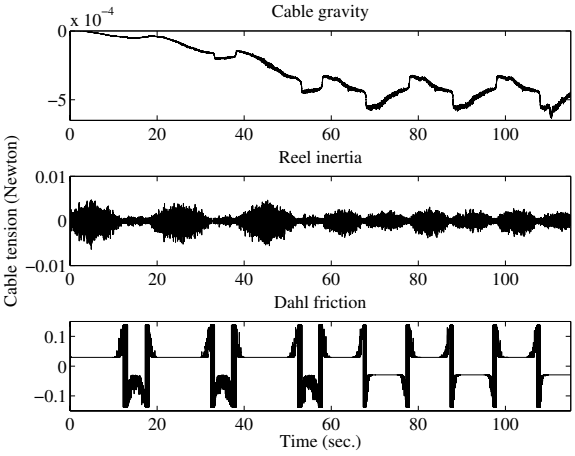

Fig. 16. Force feed-forward compensation with low angular velocity

friction model uses high values of Coulomb static and dynamic friction coefficients. Instability is generated by the cable vibration and tension measurements. As the angular velocity noise increases, so does cable vibration and then the cable tension measure could decrease toward zero, a pathological case where the cable tension control diverges.

C. Stability analysis of the hybrid control

The continuities between the solution of both control types is implemented with simple adaptitive PIDF where both accumulated values of the integral (or simply the integral value) are updated by (36) and (37) at each computation step. The demonstration of the stability is shown in Fig. 17 when (36) and (37) are used or not used for one reel. This demonstration is done when the platform is trying to leave its workspace and stays at the boundary of the workspace. The instability comes from the accumulated energy inside the PIDF when the transfert function to control is changed (standard motor position control and cable tension control).

$$\int e_t dt = I_t/s_p \quad (36)$$

$$\int e_p dt = I_p/s_t \quad (37)$$

VII. Conclusion

This paper proposes solutions for compensating non-ideal behaviour of a motorized reel. Controlling cable tension is one of the most challenging tasks for reproducing precise haptic interaction with virtual objects. The tensions in all cables are responsible to reproduce a precise pose in the virtual environnement and are responsible for generating a precise wrench. The transparency is achieved when all the reels can generate the same response with a minimum settling time as the tension controller approaches a unit gain.

The results presented in this paper suggest that some parameters should be optimized for the design of a motorized reel used in haptic applications:

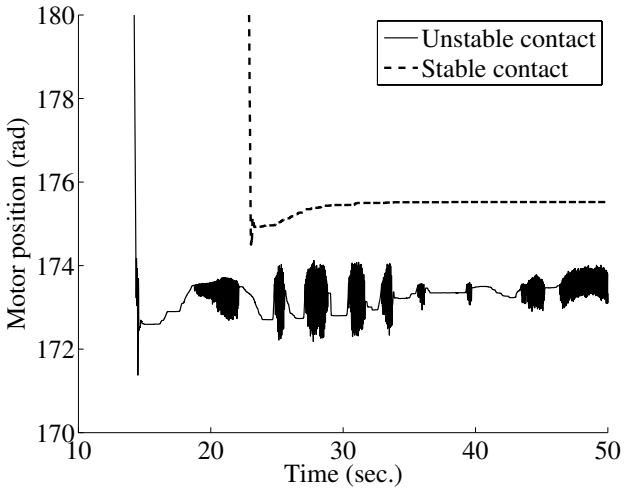

Fig. 17. Stability of position/tension hybrid control with and without integration values update

- increase stiffness of the system (reel and overall structure) to avoid control instability;
- increase frequency response for simulating rigid contact and high dynamics movement with the conservation of momentum;
- increase precision in angular velocity measurement by using tachymeter like in [31] or precise quadrature encoder to adequatly compensate friction or inertia;
- decrease the friction hysteresis to measure cable tension adequately and to avoid sticking of cable on reel parts at low velocity by minimizing (29) and
- optimize the controller for limiting overshoot and for reducing settling time with (35).

The transparency is thus studied for the static case with (29) in section IV-E and the dynamic case with (35) in section V-C. In the static case, the criterion is based on the well known Weber's law. For the dynamic case, the ES-Tuning is used with a relative cost function for finding an optimal controller in function of the cable length.

Furthermore, this paper demonstrates a stable hybrid control at the articular level of the CDLI. The tension controller includes two adaptative terms : the integrator coefficient and the accumulated value of the integral (or simply the integral value). The law governing the integrator term is designed in function of the cable length as the cable tension does not affect significatively the reel bandwidth. The accumulated value of the integral is adjusted by for the achieving stability of the hybrid command.

VIII. Future Work

The procedure for analyzing overall transparency will include a 6DDL wrench sensor installed on the haptic platform for measuring residual wrench applied by the tension controller when impendance control is selected for a null force command (the platform moves freely in the space). The wrench sensor used as the error measure for a null force command eliminates static friction at each reel by applying the highest gain possible (constraint by a margin and phase stability) on this error. The OTD algorithm then distributes this value over all the reels for precise Cartesian displacement without perturbations caused by the inertia, gravity, friction, cable real behaviour and mechanical plastic deformation such that the mechanism (the haptic foot platform and the reels) is completely transparent to the user.

References

[1] S. Perreault and C. Gosselin, "Cable-driven parallel mechanisms: application to a locomotion interface," *Journal of Mechanical Design, Transactions of the ASME*, vol. 130, no. 10, pp. 102 301–1–8, 10 2008.

[2] M. J.-D. Otis, M. Mokhtari, C. Du Tremblay, D. Laurendeau, F.-M. De Rainville, and C. M. Gosselin, "Hybrid control with multi-contact interactions for 6dof haptic foot platform on a cable-driven locomotion interface," in *Symposium on Haptics Interfaces for Virtual Environment and Teleoperator Systems 2008 - Proceedings, Haptics*, Piscataway, NJ 08855-1331, United States, 2008, pp. 161 – 168.

[3] J. E. Colgate and J. M. Brown, "Factors affecting the z-width of a haptic display," in *Proceedings of the IEEE International Conference on Robotics and Automation*, vol. 4, San Diego, CA, USA, 05 1994, pp. 3205 – 3210.

[4] R. Adams, D. Klowden, and B. Hannaford, "Stable haptic interaction using the excalibur force display," in *Proceedings of the IEEE International Conference on Robotics and Automation*, vol. 1, San Francisco, CA, USA, 2000, pp. 770 – 5.

[5] I. Ebert-Uphoff and P. Voglewede, "On the connections between cable-driven robots, parallel manipulators and grasping," in *Proceeding of the IEEE International Conference on Robotics and Automation*, vol. 5, New Orleans, LA, USA, 2004, pp. 4521 – 6.

[6] C. Bonivento, A. Eusebi, C. Melchiorri, M. Montanari, and G. Vassura, "Wireman: a portable wire manipulator for touch-rendering of bas-relief virtual surfaces," in *Proceeding of the 8th International Conference on Advanced Robotics*, Monterey, CA, USA, 1997, pp. 13 – 18.

[7] K. Kozak, Q. Zhou, and J. Wang, "Static analysis of cable-driven manipulators with non-negligible cable mass," *IEEE Transactions on Robotics*, vol. 22, no. 3, pp. 425 – 33, 06 2006.

[8] E. Ottaviano, "A system for tension monitoring in cable-based parallel architectures," in *Proceedings of the 12th IFToMM World Congress*, Besançon, France, 06 2007.

[9] F. Ferlay and F. Gosselin, "A new cable-actuated haptic interface design," in *Lecture Notes in Computer Science (including subseries Lecture Notes in Artificial Intelligence and Lecture Notes in Bioinformatics)*, vol. 5024 NCS, Heidelberg, D-69121, Germany, 2008, pp. 474 – 483.

[10] X. Diao and O. Ma, "Vibration analysis of cable-driven parallel manipulators for hardware-in-the-loop contact-dynamics," in *Proceedings of the ASME International Design Engineering Technical Conferences & Computer and Information in Engineering Conference*, Las Vegas, NV, September 2007.

[11] C. F. Baicu, C. D. Rahn, and B. D. Nibali, "Active boundary control of elastic cables: Theory and experiments," *Journal of Sound and Vibration*, vol. 198, no. 1, pp. 17 – 26, 1996.

[12] T. Kabayashi and Y. Takahashi, "Vibration control for two dimensional wire driven positioning robot," in *Proceedings of the 37th SICE Annual Conference*, Tokyo, Japan, 1998, pp. 869 – 74.

[13] M. Hiller, S. Fang, S. Mielczarek, R. Verhoeven, and D. Franitza, "Design, analysis and realization of tendon-based parallel manipulators," *Mechanism and Machine Theory*, vol. 40, no. 4, pp. 429 – 445, 2005.

[14] J. Yoon and J. Ryu, "A novel locomotion interface with two 6-dof parallel manipulators that allows human walking on various virtual terrains," *International Journal of Robotics Research*, vol. 25, no. 7, pp. 689 – 708, 07 2006.

[15] V. Duchaine and C. M. Gosselin, "Investigation of human-robot interaction stability using lyapunov theory," in *Proceedings - IEEE International Conference on Robotics and Automation*, Piscataway, NJ 08855-1331, United States, 2008, pp. 2189 – 2194.

[16] B. Hannaford and J.-H. Ryu, "Time-domain passivity control of haptic interfaces," *IEEE Transactions on Robotics and Automation*, vol. 18, no. 1, pp. 1 – 10, 2002.

[17] S. Fang, D. Franitza, M. Torlo, F. Bekes, and M. Hiller, "Motion control of a tendon-based parallel manipulator using optimal tension distribution," *IEEE/ASME Transactions on Mechatronics*, vol. 9, no. 3, pp. 561 – 8, 9 2004.

[18] D. Theodorakatos, E. Stump, and V. Kumar, "Kinematics and pose estimation for cable actuated parallel manipulators," in *Proceedings of the ASME International Design Engineering Technical Conferences and Computers and Information in Engineering Conference*, vol. 8 PART B, Las Vegas, NV, United States, 2008, pp. 1053 – 1062.
[19] M. J.-D. Otis, S. Perreault, T.-L. Nguyen-Dang, P. Lambert, M. Gouttefarde, D. Laurendeau, and C. M. Gosselin, "Determination and management of cable interferences between two 6-dof foot platforms in a cable-driven locomotion interface," *IEEE Transaction on Systems, Man and Cybernetics, Part A*, in press.
[20] F. Janabi-Sharifi, V. Hayward, and C.-S. Chen, "Discrete-time adaptive windowing for velocity estimation," *IEEE Transactions on Control Systems Technology*, vol. 8, no. 6, pp. 1003 – 1009, 11 2000.
[21] J. Canny, "A computational approach to edge detection," *IEEE Transactions on Pattern Analysis and Machine Intelligence*, vol. PAMI-8, no. 6, pp. 679 – 98, 11 1986.
[22] C. C. de Wit, H. Olsson, K. Astrom, and P. Lischinsky, "New model for control of systems with friction," *IEEE Transactions on Automatic Control*, vol. 40, no. 3, pp. 419 – 425, 1995.
[23] R. Kelly and J. Llamas, "Determination of viscous and coulomb friction by using velocity responses to torque ramp inputs," *IEEE International Conference on Robotics and Automation*, vol. 3, pp. 1740–1745, 1999.
[24] F.-J. Elmer, "Nonlinear dynamics of dry friction," *Journal of Physics A: Mathematical and General*, vol. 30, no. 17, pp. 6057–6063, 1997.
[25] R. G. Lanzara, "Weber's law modeled by the mathematical description of a beam balance," *Mathematical Biosciences*, vol. 122, no. 1, pp. 89 – 94, 1994.
[26] V. Duchaine and C. M. Gosselin, "General model of human-robot cooperation using a novel velocity based variable impedance control," in *Second Joint EuroHaptics Conference and Symposium on Haptic Interfaces for Virtual Environment and Teleoperator Systems, World Haptics 2007*, Piscataway, NJ 08855-1331, United States, 2007, pp. 445 – 451.
[27] W.-X. Ren, G. Chen, and W.-H. Hu, "Empirical formulas to estimate cable tension by cable fundamental frequency," *Structural Engineering and Mechanics*, vol. 20, no. 3, pp. 363 – 380, 2005.
[28] J.-C. Shen and H.-K. Chiang, "Pid tuning rules for second order systems," in *The 5th Asian Control Conference*, vol. 1, Melbourne, Australia, 7 2004, pp. 472–477.
[29] N. J. Killingsworth and M. Krstic, "Pid tuning using extremum seeking: Online, model free-performance optimization," *IEEE Control Systems Magazine*, vol. 26, no. 1, pp. 70 – 79, 2006.
[30] M. J.-D. Otis, T.-L. Nguyen-Dang, D. Laurendeau, and C. Gosselin, "Extremum seeking tuning for reel tension control in haptic application," in *Proceedings of the 2nd Mediterranean Conference on Intelligent Systems and Automation*, Zarzis, Tunesie, 03 2009.
[31] S. Shimano, M. Shiono, and K. Ohnishi, "Estimation of acceleration by an ac tachogenerator and its applications to servo control," *Electrical Engineering in Japan*, vol. 110, no. 6, pp. 90 – 7, 1990.

Martin J.D. Otis received the B. Eng. degree in Electrical Engineering from the Université de Sherbrooke, Québec, QC, Canada in 2002. He has worked in the GRAMS research group (*Groupe d'appareillage médical de Sherbrooke*) where he obtains a Master degree in 2004. Since 2005, he is working with the CVSL (*Computer Vision and Systems Laboratory*) and the *Laval University Robotics Laboratory* for obtaining a Ph.D. degree. He has worked as the manager of the Laval University Aerospace Team (GAUL) for two years. His research interests include the locomotion and propulsion system. However, his principal interest concerns biomedical applications where robotic systems can help physicians or practicians in the rehabilitation field.

Denis Laurendeau (M'81) holds a Bachelor's degree in Engineering Physics (1981) and a M.Sc. degree (1983) and Ph.D. degree (1986) in Electrical Engineering from Laval University, Quebec City, Quebec, Canada.

He is currently PROFESSOR in the Department of Electrical and Computer Engineering at Laval University, Quebec City, Quebec, Canada. In 2005, he spent 6 months as a VISITING SCIENTIST at Defense Research and Development Canada - Valcartier. In 2001, he spent 6 months at ABB-Bomem as PROJECT LEADER in the field of Fourier Transform Spectrometry for space applications. In 1987 he was a VISITING SCIENTIST at Hydro-Quebec Research Institute (IREQ). His research interests include computer vision, 3-D modeling for Virtual Reality, simulation in VR, object tracking, and biomedical applications of computer vision.

Dr. Laurendeau is member of the Ordre des ingénieurs du Québec (OIQ), the Canadian Image Processing and Pattern Recognition Society (CIPPRS), and the International Association for Pattern Recognition (IAPR) for which he is currently secretary of the executive committee.

Clément Gosselin received the B. Eng. degree in Mechanical Engineering from the Université de Sherbrooke, Québec, Canada, in 1985, at which time he was presented with the Gold Medal of the Governor General of Canada. He then completed a Ph.D. at McGill University, Montréal, Québec, Canada and received the D. W. Ambridge Award from McGill for the best thesis of the year in Physical Sciences and Engineering in 1988.

In 1988 he accepted a post-doctoral fellowship from the French government in order to pursue work at the Institut National de Recherche en Informatique et en Automatique (INRIA) in Sophia-Antipolis, France for a year. In 1989 he was appointed by the Department of Mechanical Engineering at Université Laval, Québec where he is now a Full Professor since 1997. He is currently holding a Canada Research Chair on Robotics and Mechatronics since January 2001. He also received, in 1993, the I. Ω. Smith award from the Canadian Society of Mechanical Engineering, for creative engineering. In 1995, he received a fellowship from the Alexander von Humboldt foundation which allowed him to spend 6 months as a visiting researcher in the Institut für Getriebetechnik und Maschinendynamik of the Technische Hochschule in Aachen, Germany. In 1996, he spent 3 months at the University of Victoria, for which he received a fellowship from the BC Advanced Systems Institute. In 1999, he also spent 2 months as a visiting professor in the Institut de Recherche en Communications et Cybernétique de Nantes (IRCCyN) in Nantes, France.

His research interests are kinematics, dynamics and control of robotic mechanical systems with a particular emphasis on the mechanics of grasping and the kinematics and dynamics of parallel manipulators and complex mechanisms. His work in the aforementioned areas has been the subject of numerous publications in International Journals and Conferences as well as of several patents. He has been an associate editor of the ASME Journal of Mechanical Design, the IEEE Transactions on Robotics and Mechanism and Machine Theory. Dr. Gosselin is a fellow of the ASME and he received, in 2008, the ASME DED Mechanisms and Robotics Committee Award for his contributions to the field.